Infrared Absorption of $Zn_{0.5}Cd_{0.5}S$ Photocatalyst Bandgap-Excited Under an Aqueous Environment

Chew, Yi-Hao

Onishi, Hiroshi

(Citation)
The Journal of Physical Chemistry C,128(11):4535-4543

(Issue Date)
2024-03-21

(Resource Type)
journal article

(Version)
Accepted Manuscript

Infrared Absorption of $Zn_{0.5}Cd_{0.5}S$ Photocatalyst Bandgap-Excited under Aqueous Environment

Yi Hao Chew[†]*, *and Hiroshi Onishi*[†‡§]*

[†]Department of Chemistry, School of Science, Kobe University, Kobe, Hyogo 657-8501, Japan

[‡]Research Center for Membrane and Film Technology, Kobe University, Kobe, Hyogo 657-8501, Japan

[§]Division of Advanced Molecular Science, Institute for Molecular Science, Okazaki, Aichi 444-8585, Japan

AUTHOR INFORMATION

Corresponding Authors

Yi-Hao Chew – *Department of Chemistry, School of Science, Kobe University, Kobe 657-8501, Japan*; orcid.org/0000-0002-8802-7608; Email: yhchew25@people.kobe-u.ac.jp

Hiroshi Onishi – *Department of Chemistry, School of Science, Kobe University, Kobe 657-8501, Japan*; orcid.org/0000-0003-1873-9105; Email: oni@kobe-u.ac.jp

ABSTRACT

The adoption of infrared and near-infrared spectrometry technique for mechanistic and kinetic studies on the photocatalytic water splitting reaction has been steadily increasing over the years. Herein, a transition metal sulfide photocatalyst, $Zn_{0.5}Cd_{0.5}S$ (ZCS), which has been proven to be an efficient hydrogen (H_2) evolution photocatalyst, was investigated through attenuated total reflection FTIR (ATR-FTIR). Electronic absorption in the wavenumber region of 500 – 3000 cm^{-1} was detected while the photocatalyst was irradiated by UV light source in a pure water environment. The source of absorption was further characterized by employing scavenging solutions, and it was found that the contribution from photogenerated electrons and holes coincidentally appeared in the same wavenumber window. This is likely to be unprecedented as prior studies generally were not able to observe electronic absorption by holes, or the holes absorption was present close to the visible wavenumber window instead. Nevertheless, the shape of absorption peak associated to holes was noticeably distinctive from that of electrons when their normalized spectra were compared, allowing easy identification of the nature of the detected absorption. These observations suggested that electrons and holes trap states were present in ZCS, and it is proposed that the trap states could be innately present due to the formation of physical defects during chemical synthesis, or they were instantaneously created upon photoexcitation where polarons were manifested by the disruption of ionic equilibrium in valence band (VB) and conduction band (CB) through injection of foreign photogenerated electrons or holes.

INTRODUCTION

Since the pioneering report by Honda and Fujishima,[1] the conversion of water into hydrogen (H_2) and oxygen (O_2) using semiconductor photocatalysts has continued to garner substantial interest over the past few decades. H_2 holds arguable more value as compared to O_2 due to it boasting a high energy content of 142 kJ/g, much higher than that of conventional fossil fuels.[2] The combustion of H_2 for energy generation also does not leave behind any carbon footprint, deeming it to be a promising source of green fuel in near future. Through photocatalytic water splitting, the process of generating H_2 is also much more environmentally friendly as compared to other developed methods such as steam reforming and electrolysis, since water and sunlight are the only two resources needed alongside the photocatalyst to kickstart the reaction. Nevertheless, this photocatalytic approach still has a glaring downside of insufficient efficiency for real-life applications at the present state of technology, despite several impressive breakthroughs reported in recent years.[3,4] In view of this, the adoption of effective analytical techniques in hope of grasping more of the underlying kinetics and mechanisms behind the photocatalytic reaction becomes imperative, so that a stronger foundation can be established for the ensuing design and modification of photocatalysts.

In-situ FTIR analysis is a technique frequently used for the detection of chemical reaction intermediates as well as unraveling of reaction pathway and mechanisms. For the analysis of water splitting reaction, things can become more intricate as the water medium tends to absorb the probing infrared (IR) light which greatly lowers the signal strength of the resultant spectrum. Attenuated total reflection (ATR) in a diamond prism comes in handy in this scenario because of its simplicity in accommodating the measurement of photocatalyst particles suspended in water (Figure 1). A number of reports have demonstrated the use of this technique for the detection of vibrational absorption arising from the intermediates involved in photocatalytic water splitting.[5–8] However, there is another important phenomenon that can be observed

through ATR-FTIR, but it has been relatively less investigated, and that is the electronic absorption spurred by photoexcited charge carriers in photocatalysts. Through comprehending the absorption signal induced by the charge carriers, scientific information such as the presence and nature of shallow states trapping the charge carriers as well as the decay kinetics of the carriers can be unveiled.[9] Hence it is believed that this piece of information should not be neglected.

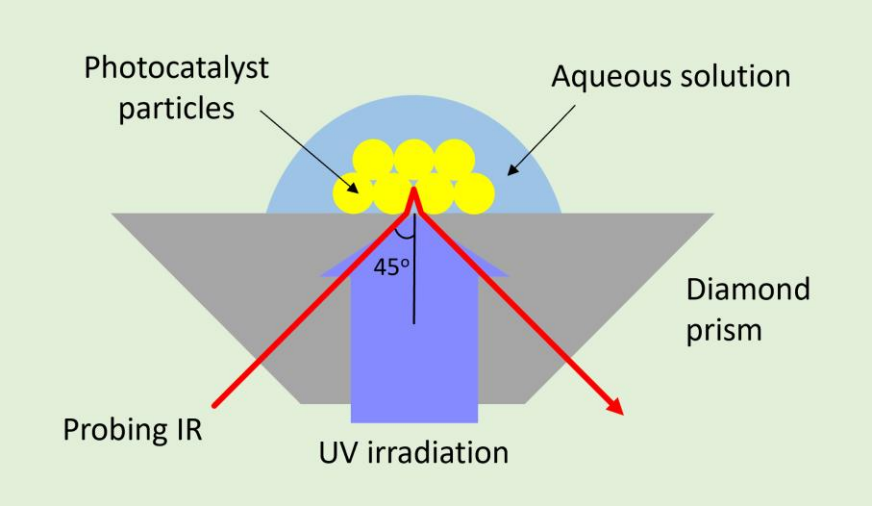

Figure 1. Diamond prism used for ATR spectroscopy.

To-date, most photocatalysts that had their electronic absorption signals studied through IR spectroscopy were oxide-based semiconductors, for instance, TiO_2,[10–16] $SrTiO_3$,[17,18] and $NaTaO_3$.[19–21] This is not surprising as oxide-based photocatalysts are known to demonstrate good activity, high robustness while also being comparably easy to synthesize. In fact, one of the most efficient water splitting photocatalytic compounds reported hitherto is based on $SrTiO_3$ with the support of co-catalysts Rh/Cr_2O_3 and CoOOH, which in turn resulting in a groundbreaking quantum efficiency of near unity.[4] Despite that, majority of the oxide-based semiconductors suffer from possessing a large bandgap, rendering them active only under illumination of short wavelength UV light.

From this perspective, sulfide-based semiconductors emerge as promising photocatalysts since they generally carry bandgaps below 2.6 eV, with the exception of ZnS.[22] Although the shortcoming of sulfides being prone to photocorrosion is undeniable, researchers have demonstrated many times the potential of sulfides as candidates for photocatalytic water splitting.[23–32] Among them, $Zn_xCd_{1-x}S$ turns out to be a popular choice owing to its tunable bandgap based on the molar ratio between Zn and Cd, which is convenient depending on the premise of photocatalytic reactions. Moreover, it has also been reported that through appropriate conditioning of the hydrothermal synthesis process, homojunctions of the zinc blende and wurtzite phases provoked by lattice disruption can be generated. It has been claimed that the presence of these homojunctions essentially created a step-like structure within its hybridized states which is conducive to prolonging the lifetime of charge carriers, thus giving rise to an enhancement in activity.[33–36] Nonetheless, despite being on the hot radar of photocatalysis, the kinetic and mechanistic aspects of the carriers fostered by illumination of $Zn_xCd_{1-x}S$ have rarely been investigated. Herein, the change in IR absorption in $Zn_{0.5}Cd_{0.5}S$ (ZCS) during UV light illumination was observed in several aqueous solutions, and the nature of the states and their formation mechanism were deliberately speculated and reported.

METHODS

Photocatalyst preparation. ZCS was synthesized through a precipitation-hydrothermal approach slightly modified from a previous report.[25] 4 mmol of zinc acetate dihydrate (99%, FUJIFILM Wako Pure Chemicals) and 4 mmol of cadmium acetate dihydrate (98%, FUJIFILM Wako Pure Chemicals) were dissolved completely in 70 mL of ultrapure water, before slowly adding in 10 mmol of thioacetamide (FUJIFILM Wako Pure Chemicals). After 30 mins of vigorous stirring, 10 mL of hydrazine monohydrate (97%, FUJIFILM Wako Pure Chemicals) was added in a dropwise manner and the mixture is further allowed to be stirred for 30 mins. Next, the resultant yellowish solution was transferred into an airtight Teflon-lined stainless-

steel autoclave, which was then placed in an oven for the hydrothermal treatment. The heating temperature was set as 190 ^{o}C and the reaction was conducted for 24 hours. After allowing the reactant to be cooled down to room temperature, the precipitate was retrieved by centrifugation and was washed two times each using ultrapure water and ethanol. The washed sample was then dried overnight at 60 ^{o}C in a drying oven.

To validate the formation of ZCS, the crystallographic structure of the resultant sample was analyzed through XRD using Rigaku Smartlab diffractometer with Cu Kα radiation. The diffraction pattern displayed multiphase characteristics, where peaks indexed to the cubic zinc blende phase and hexagonal wurtzite phase were observed and marked accordingly in Figure S1. The morphology of ZCS was also inspected through FE-SEM (JEOL JSM-7500F), and it was found that the ZCS particles have an average diameter of 20-80 nm, as seen in Figure S2. Both characterizations tallied with the results acquired in the previous works.[25,34]

ATR spectroscopy. The ATR assembly used in this study comprises of a diamond prism manufactured by Jasco. As presented earlier in Figure 1, the illustrated configuration is different from the vast majority of other reports in similar field of study, such that the excitation-triggering light source is illuminated on the same surface probed by IR beam. The incident angle of the probing IR was fixed at 45^{o} from the normal of the reflection plane, whereas the UV light was guided perpendicularly to the plane from the bottom. Both light pass through the 1.8 mm diameter reflection plane and fall directly on the sample placed on top of the plane. The depths of IR (wavenumber: 1000 cm^{-1}) light penetration into water was estimated to be 1.5 μm based on the refractive indices of diamond and water which are 2.38 and 1.32 respectively.[37] The assembly was set in a Fourier transform infrared spectrometer (FT/IR-6600, Jasco), in which a He-Ne laser light was used to irradiate the reflection plane for interferometer calibration. In this study, IR absorption in the 9000 – 500 cm^{-1} wavenumber region was measured (results were only presented from 6000 – 500 cm^{-1} instead as there were

no responses detected in 9000 – 6000 cm^{-1} region), and for this purpose, a ceramic light source and a mercury-cadmium-telluride (MCT) detector were deployed. With a wavenumber resolution of 16 cm^{-1}, 64 rounds of measurements were collected and averaged to obtain the final spectrum. The total acquisition time was about 30 seconds per spectrum.

For each set of IR absorption measurement, the sample was first placed onto the reflection plane such that it is sufficient to cover the light irradiation window completely. 300 μL of liquid was dropped onto the sample, followed by lowering the press to tighten the sample for a better result acquisition. A spectrum was then collected in the dark to serve as the background. Next, a light-emitting diode (LED) with 365 nm center wavelength (M365L3, Thorlabs) which was used as the light source for bandgap excitation was switched on to irradiate the sample for 1 minute, allowing the signals to reach a steady state. The UV light power density on the reflection plane was calibrated using a photodiode sensor (PD-300, Ophir) to be 3600 Wm^{-2}. The change in absorption spectrum (Δabsorption) was then collected for evaluation. In between acquisition sets where different solution was used, the reflection plane was carefully wiped with ethanol and conditioned with the next solution to minimize the undesirable effect from any remaining impurities. Note that all measurements were conducted in open air, and the concentrations of sacrificial reagents, namely L(+)-Ascorbic acid (99.6%, FUJIFILM Wako Pure Chemicals) and $FeCl_3$ (99% iron (III) chloride hexahydrate, Junsei Chemical), were standardized to be 0.05 M.

RESULTS AND DISCUSSION

IR absorption of ZCS in H_2O and D_2O. ZCS immersed in pure water was first placed on the ATR crystal and analyzed for its changes in absorbance (Δabsorbance) spectrum with UV light illumination. From the resultant spectra presented in Figure 2 (a), it was observed that an absorption peak emerged at the 2000-750 cm^{-1} region when the excitation UV light source was

turned on. This peak quickly subsided once the light was turned off. The shape of this peak appeared to be asymmetrical with the absorption maximum at about 950 cm^{-1}. These observations point towards a deduction where the change in absorption band was brought upon by the charge carriers that were photogenerated when ZCS was subjected with UV light. As ZCS synthesized for this study possesses a bandgap of 2.36 eV,[25] theoretically it is not possible for it to absorb the probing IR light. However, if a shallow trap state is present in ZCS during light irradiation, the charge carriers which are temporarily trapped before recombination occurs can promptly utilize the probing IR light energy and re-excite back to a higher level of unoccupied energy band. This phenomenon is thus reflected in the IR Δabsorbance spectrum, in which the energy level of such trap state in the photocatalyst can be estimated through the wavenumber position of the absorption band. Further details will be discussed comprehensively later in this manuscript. Hereby, the term 'electronic absorption' is introduced to represent this phenomenon, and it will be used recurrently throughout this manuscript.

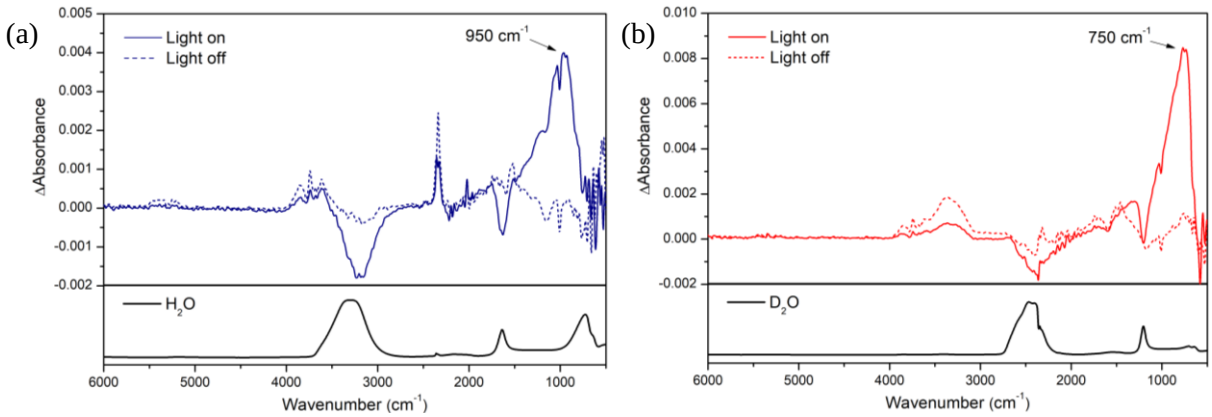

Figure 2. ΔAbsorbance spectra of ZCS immersed in (a) H_2O and (b) D_2O. The solid and dotted lines represent the spectra acquired with and without light irradiation, respectively. The absorption bands of pure H_2O and D_2O were also included at the bottom of (a) and (b) correspondingly as a reference.

Besides the apparent peak in 2000-750 cm^{-1} region, negative peaks superimposed at ~3180 and ~1650 cm^{-1} were also noticed. These can be associated to the inevitable bleaching effect

imposed by UV illumination on the vibrational absorption of water, namely O-H stretching mode and H-O-H bending mode correspondingly. Similar observations were also reported in prior works.[19,20]

To further testify this, the same measurement was conducted by using D_2O in place of H_2O, and the result is showed in Figure 2 (b). As expected, negative peaks were observed at lower wavenumber of ~2480 and 1200 cm^{-1} where the O-D stretching and D-O-D bending mode are typically found. An additional positive peak also emerged at the same region as the O-H stretching mode (~3250 cm^{-1}), and it can be ascribed to either the remaining water component adsorbed on ZCS, or atmospheric water vapor infringing through the probing volume. On the other hand, electronic absorption was also clearly observed in D_2O, however interestingly the band has a peak at slightly lower wavenumber in D_2O as compared to when ZCS was immersed in H_2O (750 cm^{-1} vs 950 cm^{-1}). Since the same ZCS was used in both cases and it is highly unlikely for D_2O to induce any changes in the electronic structure of ZCS, the depth of trap states should technically remain the same. Therefore, the charge carriers should also have similar electronic properties and should not result in such distinctive changes in the peak position.

Considering that liquid H_2O has a third characteristic absorption band of librational motions at ~750 cm^{-1}, it is suspected that intense bleaching also occurred at this position. As a result, negative peak similar to the ones at 3180 and 1650 cm^{-1} was coincidentally superimposed onto the electronic absorption peak of ZCS in H_2O, consequently instilling a ‘peak shift’ towards 950 cm^{-1}. In contrast, since the libration band of D_2O is at an even lower wavenumber region outside of the range in this work, the full electronic absorption band was displayed without any interruption from bleaching. Since the peaks in both H_2O and D_2O resemble with each other, it is believed that both responses arose from the same source, and thus both spectra can be used interchangeably depending on one’s need. Meanwhile, the nature of these carriers, whether are

they electrons or holes, is not possible to be identified by merely using water or D_2O as the liquid medium. Scavenger solutions are employed next with the aim to configure them.

IR absorption in scavenger solutions. Figure 3 (a) presents the spectra obtained when ZCS was immersed in solutions of ascorbic acid (AA) and iron (III) chloride ($FeCl_3$), in which they served as hole scavenger and electron scavenger respectively. The spectrum observed in pure water is included for comparison purposes. In AA aqueous solution, the photogenerated holes are prone to be consumed by AA, resulting in a prolonged lifetime of photoexcited electrons which are temporarily residing either in the conduction band or in the shallow trap states present in ZCS. This increases the amount of electrons that can absorb probing IR light and in turn translating to a larger Δabsorbance as compared to when pure water was used, as elucidated in Figure 3 (a). From this observation, it can be tentatively deduced that this peak is associated to photoexcited electrons instead of holes, since the holes should have been consumed by AA.

When $FeCl_3$ solution was employed, surprisingly an electronic absorption peak with greatly enhanced intensity – much stronger as compared to AA and water – appeared at similar low wavenumber region when the illuminating light source was turned on. This contradicts with the deduction that has just been made, as the presence of $FeCl_3$ as an electron scavenger is expected to remove most of the photoexcited electrons and thus an electronic absorption band associated to these electrons is bound to not occur. In a previous study conducted by Fu et al.,[19] it was also reported that the usage of methanol and Na_2SO_3 (both holes scavenger) in similar assessment of their Sr-doped $NaTaO_3$ photocatalyst resulted in an enhancement of such electronic absorption peak, but when $FeCl_3$ and $NaIO_3$ (both electrons scavenger) were used, the peak completely disappeared, proving that the peak that they acquired can be evidently ascribed to the bandgap-excited electrons.

Through a closer look into Figure 3 (a), it was observed that the absorption band formed in $FeCl_3$ solution has a noticeable wider shoulder as compared to the bands acquired in AA and water. The shape difference becomes more apparent by normalizing the absorption peaks in the region of 500 – 2900 cm^{-1} to the same maximum as plotted in Figure 3 (b). The absorption bands obtained in AA and water appear to have similar shape to each other, whereas the band in $FeCl_3$ appears relatively broader. Based on this observation, it is suspected that the distinctive band feature is an implication of the difference in nature of the photogenerated charge carriers, such that the broader absorption band represents the holes, while the narrower band is a contribution from electrons. It is not the first time this phenomenon is discovered; in fact, a report by Yamakata et al. showed that the width of electronic absorption bands assigned to photogenerated electrons and holes are evidently different in $LaTiO_2N$ photocatalyst.[17] Despite so, the bands exhibited by electrons and holes usually fall onto two separate regions, and this is a huge contrast to the findings from the present study. Considering the distinctive properties of different photocatalyst, it is proposed that ZCS demonstrated an unprecedented electronic absorption where the peaks associated to photogenerated electrons and holes coincidentally appeared at the same wavenumber window albeit having dissimilar spectral widths. Moreover, as the band shape in pure water resembles to that when AA was used, this also infers that the behavior of pure water when ZCS was employed as photocatalyst inclines towards it being a holes scavenger, despite that theoretically water can be reduced and oxidized simultaneously by ZCS due to the bandgap of ZCS enveloping both water reduction and oxidation potentials. Essentially, it obliquely implies that the oxidation of water by ZCS is more prone to occur in a pure water environment without any external scavengers. This is an interesting deduction since ZCS has rarely been studied on its water oxidation activity, hence other supporting characterizations will need to be done in the future to validate this speculative statement.

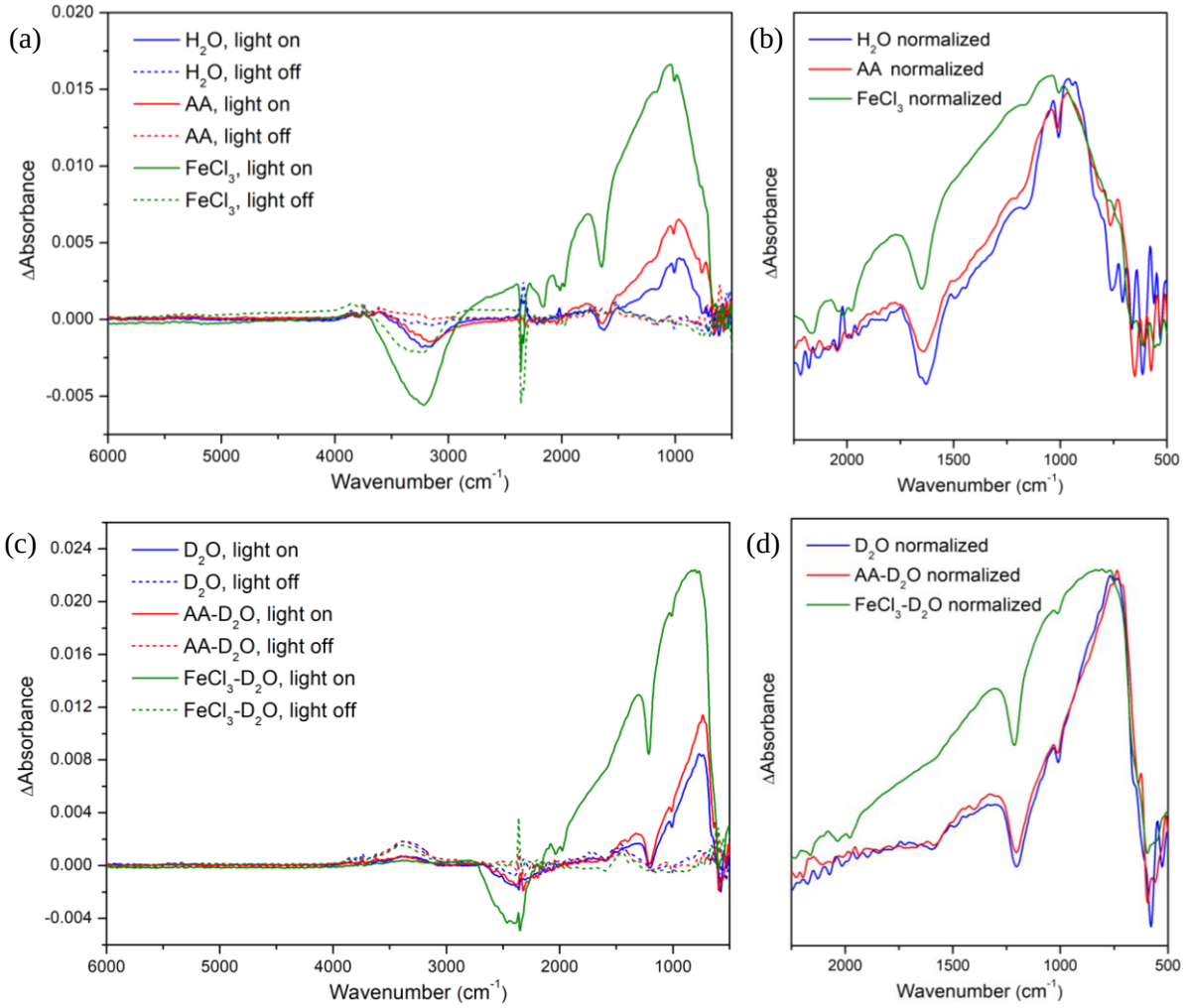

Figure 3. ΔAbsorbance spectra of ZCS immersed in sacrificial solutions prepared with (a) H_2O and (c) D_2O. (b) and (d) are the respective normalized spectra of (a) and (c). The solid and dotted lines represent the spectra acquired with and without light irradiation correspondingly.

To verify the consistency of the present findings, similar measurements were performed with the D_2O counterparts of each scavenger, namely AA dissolved in D_2O (AA-D_2O) and $FeCl_3$ dissolved in D_2O ($FeCl_3$-D_2O). The result compiled in Figure 3 (c) showed a same trend as that when water was used, where pure D_2O has the lowest peak intensity, followed by AA-D_2O and $FeCl_3$-D_2O accordingly. Without the bleaching effect of UV on the vibrational absorption of water which was elaborated earlier, all peaks were present at a lower wavenumber region of ~750 cm^{-1}. By comparing the normalized peaks in Figure 3 (d), the band obtained in $FeCl_3$-D_2O also tallied with the prior set of results that were acquired in water-based solutions, in

which it stood out with a much broader spectral shoulder among all spectra. As a side note, small peaks that appeared at ~3250 cm^{-1} and ~1450 cm^{-1} can be ascribed to O-H stretching mode arising from H_2O adsorbed on ZCS and H-O-D bending mode from the trace amount of HDO in the D_2O solution, respectively.[38]

Additionally, through Figure 3 (a) and (c), the electronic absorptions of ZCS in both variations of $FeCl_3$ solutions (H_2O and D_2O-based) exhibited the strongest intensity, far ahead of the spectra taken in AA (AA-D_2O) or H_2O (D_2O). It has been widely accepted that a strong absorption in this context signifies the relatively high quantity of charge carriers that are able to absorb the corresponding IR energy, even though the factors that affect this quantity can vary from case to case. Here, it is apparent that the contribution from photogenerated holes was substantially higher and this could be related to the scavenging ability of $FeCl_3$ when paired with ZCS. In general, certain classes of photocatalytic materials have their 'preferred' scavenging solution where the resultant product yields are maximized due to the excellent scavenging abilities of the respective solutions. For example, thioacetamide (TEOA) as the best-in-slot (BIS) holes scavenger for g-C_3N_4 polymeric photocatalyst,[39–41] Na_2S/Na_2SO_3 or AA as the BIS holes scavenger for sulfide-based photocatalysts in which one may provide better outcome over another depending on the co-catalysts used,[42–45] $Na_2S_2O_8$ as electron scavenger for ferrites such as $NiFeO_x$ and $BiFeO_3$,[46,47] and $AgNO_3$ or $FeCl_3$ as the more generic go-to electron scavenger in many of the studies using the popular oxygen evolution photocatalysts, WO_3 and $BiVO_4$.[48–54] As the usage of ZCS for oxygen evolution is rather scarce, the combination of ZCS and $FeCl_3$ as the photocatalyst-electron scavenger pair has most likely not been assessed before. Considering the occasion where $FeCl_3$ has great synergy with ZCS and can effectively draw away the photoexcited electrons in ZCS, this will leave a substantial amount of holes in the valence band (VB) of ZCS that can thus contribute to strong electronic absorption during ATR-FTIR assessment as evidently protrayed in Figure 3 (a) and (c).

IR Absorption mechanism. Upon breaking down of the electronic absorption spectra that were successfully observed on ZCS in 3 different liquid environments, it is also important to dive deeper into the mechanism of these absorptions. As mentioned briefly before, these IR absorptions that occurred during light irradiation indicates the presence of shallow trap states. The photogenerated electrons (or holes) that were trapped momentarily in the trap states absorbed the probing IR beam to get re-excited to CB (or VB), hence exhibiting a response in the IR absorption spectrum. From a classic semiconductor point of view, trap states are often caused by the presence of physical defects which are introduced through modifications, for instance interstitial or substitutional doping of foreign atoms and stripping of local atoms resulting in atomic vacancies. Aside from that, it is also generally accepted that natural crystalline defects are inevitable during materials synthesis especially in wet-chemical procedures. In this study, the pristine ZCS photocatalyst used was synthesized via hydrothermal method without any form of additional modifications, thus it is safe to assume that any physical trap states present were results of inevitable natural defects that were induced during synthesis. In fact, in accordance with the observations in Section 3.2, these natural defects have fostered traps in close vicinity of both VB and CB as electronic absorption associated to both electrons and holes were observed.

Apart from the physical defect theory, the origin of the trap states can also be interpreted from the viewpoint of polarons. Here, the injection of charges into CB (or removal from VB) during photoexcitation instigated temporal dislocation of ionic atoms from their equilibrium positions due to polarizing effect, and this invokes Coulombic potential well that traps the photoexcited electrons (or holes). Such quasiparticle constituting of the foreign charged particle and its interaction with surrounding atoms is commonly known as a polaron. Contrasting to the physical defect theory where the trap states already exist in the crystal structure of ZCS prior to photoexcitation, the polaronic effect theory inferred that the traps are instantaneously self-

induced by the photogenerated charge carriers the moment when bandgap excitation is triggered. These traps are expected to fade off when the excitation light is turned off as the ionic atoms will return to their original equilibrium state. A sample illustration elucidating this occurrence and the self-trapping mechanism for photoexcited electrons is hereby included in Figure 4.

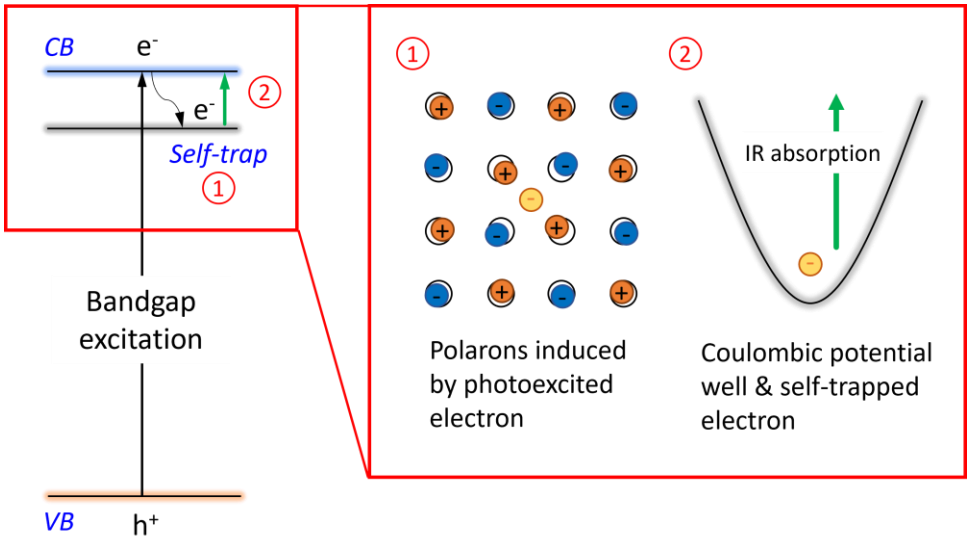

Figure 4. Self-trapping of electrons due to polaronic effect during photoexcitation. This illustration gives an example from the electrons perpective. Similar mechanism is applicable to holes at VB.

Following the two possible mechanisms of trap states formation, the attention is then shifted towards a striking feature in all absorption bands that were acquired, that is the asymmetry of the peaks. When a trap state is postulated to be present in the crystal structure of a photocatalyst, it is often regarded to be a state positioned on a discrete energy level, such that any movement of electrons (holes) between the trap and VB (CB) will require absorption of energy exactly equivalent to the energy gap between the two levels. As such, theoretically a symmetrical peak should be reflected in the IR absorption spectrum which is not the case here as seen in Figure 3. In fact, the asymmetrical bands with peaks that are skewed towards the lower wavenumber

region suggest otherwise. Although the circumstance here can be ambiguous without further supporting evidence, one of the most probable reasons should be the formation of heterogeneous trap states, as depicted in Figure 5. For the case of physical traps, several levels of trap states can simply be formed just because the precise control of defects induction is usually not possible during synthesis. On another hand, when the polarons-induced traps are taken into consideration, different sizes of polarons may be manifested and it results in varied depth of Coulombic potential wells in which the charge carriers are trapped in. In either scenario, the energy level with the highest population of traps should be consistent with the position of the absorption peak, for instance 0.093 eV below the CB for electron traps (peak position of 750 cm^{-1} from the narrower bands) and 0.10 eV above the VB for hole traps (peak position of 800 cm^{-1} from the wider band), both enumerated from Figure 3 (c). As the energy gap increases, some trap states are also present, but the density of traps decreases correspondingly, therefore resulting in the skewed spectra.

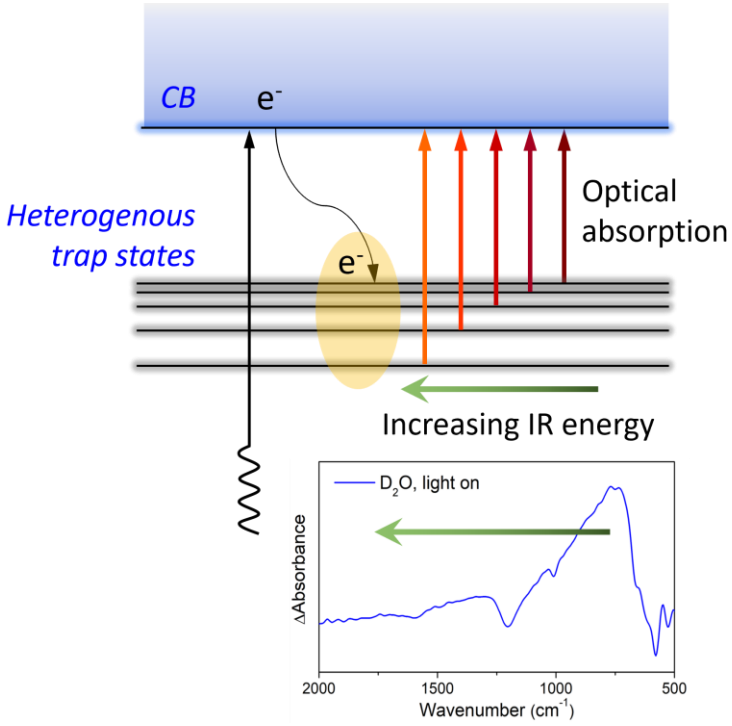

Figure 5. Electrons trapped in the heterogenous trap states absorbing different IR energy to be re-excited to CB. Similar interpretation can be applied for the holes at VB.

Another postulation for the skewed spectra lays in the absorption of additional IR energy that enables the trapped charge carriers to move from their spatially localized states into the unbound continuum states within the CB or VB while facilitated by phonons. This can occur regardless of whether the charges are accommodated in physical defects or the ground states of the polaronic potential wells, and the resultant optical absorption band usually appears asymmetric.[55] Normally, the initial states of these carriers are confined in real space and its momentum is limited. Along with the absorption of photon energy, there are chances for the optical transition of carriers from the trap states into the CB (or VB) continuum, albeit the probability is however dependent on the electron momentum required to reach the final state delocalized in space. Since this momentum is provided by phonons in the host lattice, statistically the phonons with higher energy are much lower in abundance as compared to phonons with lower energy, hence the chances for charge carriers to transition into a deeper unbound state are lower. From this context, the low energy threshold of the absorption is determined by the energy gap between the trap state and the bottom of the continuum state. This generates a peak near the threshold, and the absorption coefficient then reduces gradually when the photon energy goes above the threshold, generating a skewed spectrum as seen in Figure 3. A scheme demonstrating this phenomenon is included as Figure 6. Note that it is possible for the heterogeneity in trap states and transition of trapped charges into unbound continuum states to occur concurrently, but for the scope of this study, the two scenarios are elaborated separately to reduce the complexity. In fact, while it is well accepted that trap states can have varied effects on the resultant photocatalytic kinetics; for instance, some might be effective temporary traps that prolong the lifetime of electrons and holes and some might be serving as recombination centres instead; from the present scope of study, it is not possible to tell the effectiveness of the traps described in the two scenarios above in terms of enhancing the efficiency of photocatalytic water splitting reaction. More in-depth studies on the kinetics

of these traps and the combined effect of both phenomena will be a noteworthy topic of research in the future especially with the aid of computational methods such as density functional theory.

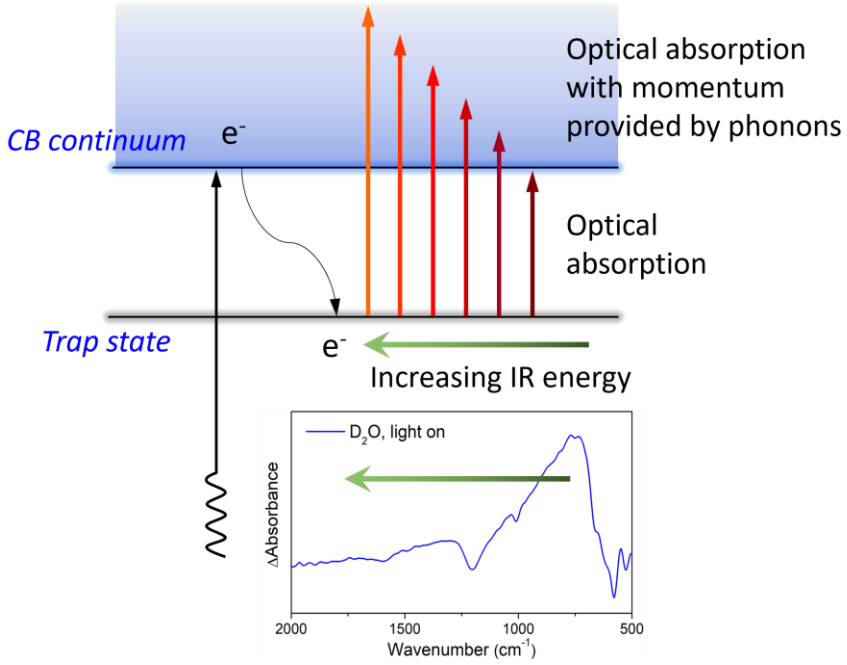

Figure 6. Electrons excited beyond the lowest unoccupied state in CB into the unbound continuum states facilitated by phonons. Similar interpretation can be applied for the holes at VB.

CONCLUSIONS

In essence, the in-situ response of IR probing on ZCS immersed in aqueous environment during photoirradiation was successfully observed and reported for the first time. The ΔAbsorbance peak that appeared only during irradiation was ascribed to electronic absorption, which reflects the phenomenon of IR energy absorption by the photogenerated charge carriers that were momentarily trapped in the respective trap states. Through measurements in scavenging solutions, it was revealed that the contribution from electrons and holes could be distinguished based on the qualitative difference of the acquired peak shape, although coincidentally both contributions appeared in a similar wavenumber window, which was unheard of prior to this

study. Specifically, the electronic absorption by photogenerated electrons in ZCS was recognized by the relatively narrower absorbance band when compared with the absorption caused by holes. With the presence of these responses, it was divulged that trap states were present in close vicinity of both valence and conduction bands. The potential origins of these traps were also laid out accordingly based on two different viewpoints. From the perspectiv of classic semiconductive materials, natural defects that were inherently formed in the lattice of ZCS during the hydrothermal synthesis process could have introduced some physical trap states. On another hand, when the photogenerated charge carriers were injected into the valence or conduction bands, polarons that were instantaneously created have also caused disruption to the surrounding ionic atoms in their originally equilibrium states, and this led to the formation of Coulumbic potential wells that can entrap the carriers. Notably, based on the asymmetry in the observed absorbance band, it was suspected that there were some heterogeneities in the trap states, in which different density of traps were introduced at multiple levels, or the possibility that the carriers gained different magnitudes of momentum from the phonons to be projected into the unbound continuum states. All in all, this study opens a new avenue for the characterization of sulfide photocatalysts by highlighting the feasibility of ATR-FTIR to analyze the photogenerated charge carriers instantaneously during light irradiation.

ASSOCIATED CONTENT

Supporting Information. The supporting information is available free of charge on the ACS publications website as a PDF.

XRD pattern (Figure S1) and FE-SEM image (Figure S2) of ZCS.

AUTHOR INFORMATION

Corresponding authors

Yi-Hao Chew – *Department of Chemistry, School of Science, Kobe University, Kobe 657-8501, Japan*; orcid.org/0000-0002-8802-7608; Email: yhchew25@people.kobe-u.ac.jp

Hiroshi Onishi – *Department of Chemistry, School of Science, Kobe University, Kobe 657-8501, Japan*; *Division of Advanced Molecular Science, Institute for Molecular Science, Okazaki 444-8585*; orcid.org/0000-0003-1873-9105; Email: oni@kobe-u.ac.jp

Author Contributions

The authors contributed to the development of the manuscript.

Notes

The authors declare no competing financial interest.

ACKNOWLEDGEMENT

This study was supported by JSPS KAKENHI (Grant number: 22H00344).

REFERENCES

(1) Fujishima, A.; Honda, K. Electrochemical Photolysis of Water at A Semiconductor Electrode. *Nature* **1972**, *238*, 37–38.

(2) Chee, M. K. T.; Ng, B.-J.; Chew, Y.-H.; Chang, W. S.; Chai, S.-P. Photocatalytic Hydrogen Evolution from Artificial Seawater Splitting over Amorphous Carbon Nitride: Optimization and Process Parameters Study via Response Surface Modeling. *Materials (Basel).* **2022**, *15*, 4894.

(3) Zhou, P.; Navid, I. A.; Ma, Y.; Xiao, Y.; Wang, P.; Ye, Z.; Zhou, B.; Sun, K.; Mi, Z. Solar-to-Hydrogen Efficiency of More Than 9% in Photocatalytic Water Splitting. *Nature* **2023**, *613*, 66–70.

(4) Takata, T.; Jiang, J.; Sakata, Y.; Nakabayashi, M.; Shibata, N.; Nandal, V.; Seki, K.; Hisatomi, T.; Domen, K. Photocatalytic Water Splitting with A Quantum Efficiency of Almost Unity. *Nature* **2020**, *581*, 411–414.

(5) Roberts, C. A.; Phivilay, S. P.; Wachs, I. E. Nature of Surface Oxygen Intermediates on TiO_2 during Photocatalytic Splitting of Water. *Chinese Chem. Lett.* **2018**, *29*, 769–772.

(6) Chen, T.; Ding, Q.; Wang, X.; Feng, Z.; Li, C. Mechanistic Studies on Photocatalytic Overall Water Splitting over Ga_2O_3-Based Photocatalysts by *Operando* MS-FTIR Spectroscopy. *J. Phys. Chem. Lett.* **2021**, *12*, 6029–6033.

(7) Zhang, M.; de Respinis, M.; Frei, H. Time-Resolved Observations of Water Oxidation Intermediates on A Cobalt Oxide Nanoparticle Catalyst. *Nat. Chem.* **2014**, *6*, 362–367.

(8) Nakamura, R.; Imanishi, A.; Murakoshi, K.; Nakato, Y. In Situ FTIR Studies of Primary Intermediates of Photocatalytic Reactions on Nanocrystalline TiO_2 Films in Contact with Aqueous Solutions. *J. Am. Chem. Soc.* **2003**, *125*, 7443–7450.

(9) Miao, T. J.; Tang, J. Characterization of Charge Carrier Behavior in Photocatalysis Using Transient Absorption Spectroscopy. *J. Chem. Phys.* **2020**, *152*, 194201.

(10) Sezen, H.; Buchholz, M.; Nefedov, A.; Natzeck, C.; Heissler, S.; Di Valentin, C.; Wöll, C. Probing Electrons in TiO_2 Polaronic Trap States by IR-Absorption: Evidence for The Existence of Hydrogenic States. *Sci. Rep.* **2014**, *4*, 3808.

(11) Savory, D. M.; McQuillan, A. J. IR Spectroscopic Behavior of Polaronic Trapped

Electrons in TiO_2 under Aqueous Photocatalytic Conditions. *J. Phys. Chem. C* **2014**, *118*, 13680–13692.

(12) Vequizo, J. J. M.; Matsunaga, H.; Ishiku, T.; Kamimura, S.; Ohno, T.; Yamakata, A. Trapping-Induced Enhancement of Photocatalytic Activity on Brookite TiO_2 Powders: Comparison with Anatase and Rutile TiO_2 Powders. *ACS Catal.* **2017**, *7*, 2644–2651.

(13) Yamakata, A.; Vequizo, J. J. M. Curious Behaviors of Photogenerated Electrons and Holes at The Defects on Anatase, Rutile, and Brookite TiO_2 Powders: A Review. *J. Photochem. Photobiol. C Photochem. Rev.* **2019**, *40*, 234–243.

(14) Yoshihara, T.; Katoh, R.; Furube, A.; Tamaki, Y.; Murai, M.; Hara, K.; Murata, S.; Arakawa, H.; Tachiya, M. Identification of Reactive Species in Photoexcited Nanocrystalline TiO_2 Films by Wide-Wavelength-Range (400-2500 nm) Transient Absorption Spectroscopy. *J. Phys. Chem. B* **2004**, *108*, 3817–3823.

(15) Shinoda, T.; Murakami, N. Photoacoustic Fourier Transform Near- and Mid-Infrared Spectroscopy for Measurement of Energy Levels of Electron Trapping Sites in Titanium(IV) Oxide Photocatalyst Powders. *J. Phys. Chem. C* **2019**, *123*, 12169–12175.

(16) Panayotov, D. A.; Burrows, S. P.; Morris, J. R. Infrared Spectroscopic Studies of Conduction Band and Trapped Electrons in UV-Photoexcited, H-Atom N-Doped, and Thermally Reduced TiO_2. *J. Phys. Chem. C* **2012**, *116*, 4535–4544.

(17) Yamakata, A.; Kawaguchi, M.; Nishimura, N.; Minegishi, T.; Kubota, J.; Domen, K. Behavior and Energy States of Photogenerated Charge Carriers on Pt- or CoO_x-Loaded $LaTiO_2N$ Photocatalysts: Time-Resolved Visible to Mid-Infrared Absorption Study. *J. Phys. Chem. C* **2014**, *118*, 23897–23906.

(18) Furuhashi, K.; Jia, Q.; Kudo, A.; Onishi, H. Time-Resolved Infrared Absorption Study of $SrTiO_3$ Photocatalysts Codoped with Rhodium and Antimony. *J. Phys. Chem. C* **2013**, *117*, 19101–19106.

(19) Fu, Z.; Hirai, T.; Onishi, H. Long-Life Electrons in Metal-Doped Alkali-Metal Tantalate Photocatalysts Excited under Water. *J. Phys. Chem. C* **2021**, *125*, 26398–26405.

(20) Fu, Z.; Onishi, H. Infrared and Near-Infrared Spectrometry of Anatase and Rutile Particles Bandgap Excited in Liquid. *J. Phys. Chem. B* **2023**, *127*, 321–327.

(21) An, L.; Onishi, H. Electron-Hole Recombination Controlled by Metal Doping Sites in

$NaTaO_3$ Photocatalysts. *ACS Catal.* **2015**, *5*, 3196–3206.

(22) Wang, J.; Lin, S.; Tian, N.; Ma, T.; Zhang, Y.; Huang, H. Nanostructured Metal Sulfides: Classification, Modification Strategy, and Solar-Driven CO_2 Reduction Application. *Adv. Funct. Mater.* **2021**, *31*, 2008008.

(23) Li, Y.; Hu, Y.; Peng, S.; Lu, G.; Li, S. Synthesis of CdS Nanorods by An Ethylenediamine Assisted Hydrothermal Method for Photocatalytic Hydrogen Evolution. *J. Phys. Chem. C* **2009**, *113*, 9352–9358.

(24) Qiu, B.; Zhu, Q.; Du, M.; Fan, L.; Xing, M.; Zhang, J. Efficient Solar Light Harvesting CdS/Co_9S_8 Hollow Cubes for Z-Scheme Photocatalytic Water Splitting. *Angew. Chemie* **2017**, *129*, 2728–2732.

(25) Chew, Y.-H.; Ng, B.-J.; Tang, J.-Y.; Tan, L.-L.; Chai, S.-P. A Synergistic Combination of P-Doped $Zn_{0.5}Cd_{0.5}S$ and CoP for Dual-Stage Electron Trapping and Its Application in Seawater Splitting. *Sol. RRL* **2021**, *5*, 2100016.

(26) Chong, W.-K.; Ng, B.-J.; Kong, X. Y.; Tan, L.-L.; Putri, L. K.; Chai, S.-P. Non-Metal Doping Induced Dual p-n Charge Properties in A Single $ZnIn_2S_4$ Crystal Structure Provoking Charge Transfer Behaviors and Boosting Photocatalytic Hydrogen Generation. *Appl. Catal. B Environ.* **2023**, *325*, 122372.

(27) Zhu, Q.; Xu, Z.; Yi, Q.; Nasir, M.; Xing, M.; Qiu, B.; Zhang, J. Prolonged Electron Lifetime in Sulfur Vacancy-Rich ZnCdS Nanocages by Interstitial Phosphorus Doping for Photocatalytic Water Reduction. *Mater. Chem. Front.* **2020**, *4*, 3234–3239.

(28) Ye, H. F.; Shi, R.; Yang, X.; Fu, W. F.; Chen, Y. P-Doped $Zn_xCd_{1-x}S$ Solid Solutions as Photocatalysts for Hydrogen Evolution from Water Splitting Coupled with Photocatalytic Oxidation of 5-Hydroxymethylfurfural. *Appl. Catal. B Environ.* **2018**, *233*, 70–79.

(29) Nadtochenko, V.; Kochev, S.; Kabachii, Y.; Kostrov, A.; Gostev, F.; Shelaev, I.; Aybush, A.; Vasin, A.; Titov, A.; Kiwi, J. Fast Kinetic Laser Spectroscopy of The Exciton Dynamics during Photocatalytic ZnCdS/ZnCdS/ZnS QDs Mediated Hydrogen Production. *Appl. Phys. A Mater. Sci. Process.* **2023**, *129*, 155.

(30) Hao, X.; Shao, Y.; Xiang, D.; Jin, Z. Photocatalytic Overall Water Splitting Hydrogen Production over ZnCdS by Spatially-Separated WP and Co_3O_4 Cocatalysts. *Sol. Energy*

Mater. Sol. Cells **2022**, *248*, 111970.

(31) Li, B.; Wang, W.; Zhao, J.; Wang, Z.; Su, B.; Hou, Y.; Ding, Z.; Ong, W.-J.; Wang, S. All-Solid-State Direct Z-Scheme $NiTiO_3/Cd_{0.5}Zn_{0.5}S$ Heterostructures for Photocatalytic Hydrogen Evolution with Visible Light. *J. Mater. Chem. A* **2021**, *9*, 10270–10276.

(32) Li, Y.; Zhu, P.; Tsubaki, N.; Jin, Z. Fabrication of Hierarchical CoP/ZnCdS/Co_3O_4 Quantum Dots (800>40>4.5 nm) Bi-Heterostructure Cages for Efficient Photocatalytic Hydrogen Evolution. *Renew. Energy* **2022**, *198*, 626–636.

(33) Liu, M.; Jing, D.; Zhou, Z.; Guo, L. Twin-Induced One-Dimensional Homojunctions Yield High Quantum Efficiency for Solar Hydrogen Generation. *Nat. Commun.* **2013**, *4*, 2278.

(34) Chew, Y.-H.; Ng, B.-J.; Kong, X. Y.; Putri, L. K.; Tang, J.-Y.; Tan, L.-L.; Chai, S.-P. Interfacial Engineering of A Zinc Blende/Wurtzite Homojunction Photocatalyst through Hybridization with A Cobalt Phosphide Co-Catalyst for Enhanced Visible-Light-Driven Photocatalytic H_2 Evolution. *Sustain. Energy Fuels* **2020**, *4*, 1822–1827.

(35) Liu, M.; Wang, L.; Lu, G.; Yao, X.; Guo, L. Twins in $Cd_{1-x}Zn_xS$ Solid Solution: Highly Efficient Photocatalyst for Hydrogen Generation from Water. *Energy Environ. Sci.* **2011**, *4*, 1372–1378.

(36) Du, H.; Liang, K.; Yuan, C. Z.; Guo, H. L.; Zhou, X.; Jiang, Y. F.; Xu, A. W. Bare $Cd_{1-x}Zn_xS$ ZB/WZ Heterophase Nanojunctions for Visible Light Photocatalytic Hydrogen Production with High Efficiency. *ACS Appl. Mater. Interfaces* **2016**, *8*, 24550–24558.

(37) Haynes, W. M. *CRC Handbook of Chemistry and Physics, 92nd Edition*; CRC Press: Boca Raton, 2011.

(38) Park, K.; Kim, Y.; Lee, K. J. Analysis of Deuterated Water Contents Using FTIR Bending Motion. *J. Radioanal. Nucl. Chem.* **2019**, *322*, 487–493.

(39) Iqbal, W.; Qiu, B.; Lei, J.; Wang, L.; Zhang, J.; Anpo, M. One-Step Large-Scale Highly Active g-C_3N_4 Nanosheets for Efficient Sunlight-Driven Photocatalytic Hydrogen Production. *Dalt. Trans.* **2017**, *46*, 10678–10684.

(40) Putri, L. K.; Ng, B.-J.; Ong, W.-J.; Lee, H. W.; Chang, W. S.; Chai, S.-P. Engineering Nanoscale p-n Junction: Via The Synergetic Dual-Doping of p-Type Boron-Doped

Graphene Hybridized with n-Type Oxygen-Doped Carbon Nitride for Enhanced Photocatalytic Hydrogen Evolution. *J. Mater. Chem. A* **2018**, *6*, 3181–3194.

(41) Chee, M. K. T.; Er, C.-C.; Tang, J.-Y.; Tan, L.-L.; Chang, W. S.; Chai, S.-P. Tuning The Electronic Band Structure of Graphitic Carbon Nitride by Breaking Intramolecular Bonds: A Simple and Effective Approach for Enhanced Photocatalytic Hydrogen Production. *Appl. Surf. Sci.* **2020**, *529*, 146600.

(42) Ng, B.-J.; Putri, L. K.; Kong, X. Y.; Shak, K. P. Y.; Pasbakhsh, P.; Chai, S.-P.; Mohamed, A. R. Sub-2 nm Pt-Decorated $Zn_{0.5}Cd_{0.5}S$ Nanocrystals with Twin-Induced Homojunctions for Efficient Visible-Light-Driven Photocatalytic H_2 Evolution. *Appl. Catal. B Environ.* **2018**, *224*, 360–367.

(43) Qi, S.; Miao, Y.; Chen, J.; Chu, H.; Tian, B.; Wu, B.; Li, Y.; Xin, B. Controlled Biosynthesis of ZnCdS Quantum Dots with Visible-Light-Driven Photocatalytic Hydrogen Production Activity. *Nanomaterials* **2021**, *11*, 1357.

(44) Ha, E.; Ruan, S.; Li, D.; Zhu, Y.; Chen, Y.; Qiu, J.; Chen, Z.; Xu, T.; Su, J.; Wang, L.; Hu, J. Surface Disorder Engineering in ZnCdS for Cocatalyst Free Visible Light Driven Hydrogen Production. *Nano Res.* **2022**, *15*, 996–1002.

(45) Mei, Z.; Zhang, B.; Zheng, J.; Yuan, S.; Zhuo, Z.; Meng, X.; Chen, Z.; Amine, K.; Yang, W.; Wang, L. W. et al. Tuning Cu Dopant of $Zn_{0.5}Cd_{0.5}S$ Nanocrystals Enables High-Performance Photocatalytic H_2 Evolution from Water Splitting under Visible-Light Irradiation. *Nano Energy* **2016**, *26*, 405–416.

(46) Ramadan, W.; Feldhoff, A.; Bahnemann, D. Assessing The Photocatalytic Oxygen Evolution Reaction of $BiFeO_3$ Loaded with IrO_2 Nanoparticles as Cocatalyst. *Sol. Energy Mater. Sol. Cells* **2021**, *232*, 111349.

(47) Nurlaela, E.; Shinagawa, T.; Qureshi, M.; Dhawale, D. S.; Takanabe, K. Temperature Dependence of Electrocatalytic and Photocatalytic Oxygen Evolution Reaction Rates Using NiFe Oxide. *ACS Catal.* **2016**, *6*, 1713–1722.

(48) Chew, Y.-H.; Tang, J.-Y.; Tan, L.-J.; Choi, B. W. J.; Tan, L.-L.; Chai, S.-P. Engineering Surface Oxygen Defects on Tungsten Oxide to Boost Photocatalytic Oxygen Evolution from Water Splitting. *Chem. Commun.* **2019**, *55*, 6265–6268.

(49) Liu, Q.; Wang, F.; Lin, H.; Xie, Y.; Tong, N.; Lin, J.; Zhang, X.; Zhang, Z.; Wang, X.

Surface Oxygen Vacancy and Defect Engineering of WO_3 for Improved Visible Light Photocatalytic Performance. *Catal. Sci. Technol.* **2018**, *8*, 4399–4406.

(50) Yang, Y.; Zhang, Q.; Yang, X.; Hu, H.; Liu, L.; Ye, J.; Wang, D. Effect of The Valence State in Co-Based Cocatalyst on The Photocatalytic Oxygen Evolution Reactivity of WO_3. *Energy and Fuels* **2022**, *36*, 11457–11466.

(51) Liu, G.; Han, J.; Zhou, X.; Huang, L.; Zhang, F.; Wang, X.; Ding, C.; Zheng, X.; Han, H.; Li, C. Enhancement of Visible-Light-Driven O_2 Evolution from Water Oxidation on WO_3 Treated with Hydrogen. *J. Catal.* **2013**, *307*, 148–152.

(52) Okunaka, S.; Tokudome, H.; Hitomi, Y.; Abe, R. Preparation of Fine Particles of Sheelite-Monoclinic Phase $BiVO_4$ via An Aqueous Chelating Method for Efficient Photocatalytic Oxygen Evolution under Visible-Light Irradiation. *J. Mater. Chem. A* **2016**, *4*, 3926–3932.

(53) Abbood, H. A.; Alabdie, A.; Al-Hawash, A.; Abbood, A. A.; Huang, K. Fabrication of Double-Sided Comb-like F/Ce Co-Doped $BiVO_4$ Micro/Nanostructures for Enhanced Photocatalytic Degradation and Water Oxidation. *J. Nanoparticle Res.* **2020**, *22*, 78.

(54) Zhou, Y.; Vuille, K.; Heel, A.; Probst, B.; Kontic, R.; Patzke, G. R. An Inorganic Hydrothermal Route to Photocatalytically Active Bismuth Vanadate. *Appl. Catal. A Gen.* **2010**, *375*, 140–148.

(55) Emin, D. Optical Properties of Large and Small Polarons and Bipolarons. *Phys. Rev. B* **1993**, *48*, 13691–13702.

TOC GRAPHIC

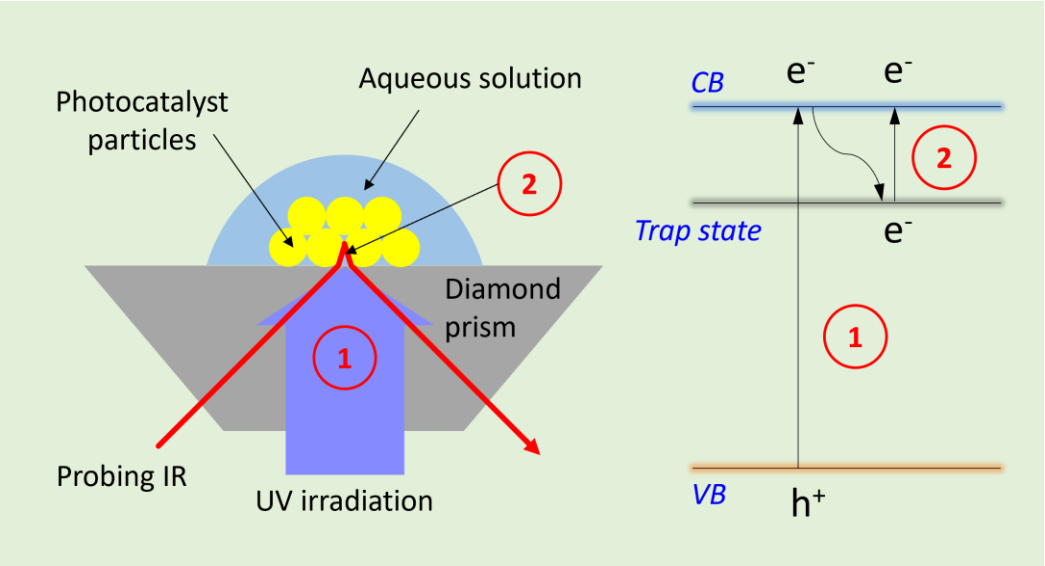
Photocatalyst particles
Aqueous solution
2
Diamond prism
1
Probing IR
UV irradiation
CB
e-
e-
2
Trap state
e-
1
VB
h+